Drugs in R&D (2025) 25:1–17
https://doi.org/10.1007/s40268-024-00495-1

ORIGINAL RESEARCH ARTICLE

Evaluation of BCRP-Related DDIs Between Methotrexate and Cyclosporin A Using Physiologically Based Pharmacokinetic Modelling

Stephan Schaller[1] · Ingrid Michon[2] · Vanessa Baier[1] · Frederico Severino Martins[1] · Patrick Nolain[3] · Amit Taneja[3,4]

Accepted: 22 October 2024 / Published online: 24 December 2024

Abstract

Background and Objective This study provides a physiologically based pharmacokinetic (PBPK) model-based analysis of the potential drug–drug interaction (DDI) between cyclosporin A (CsA), a breast cancer resistance protein transporter (BCRP) inhibitor, and methotrexate (MTX), a putative BCRP substrate.

Methods PBPK models for CsA and MTX were built using open-source tools and published data for both model building and for model verification and validation. The MTX and CsA PBPK models were evaluated for their application in simulating BCRP-related DDIs. A qualification of an introduced empirical uniform in vitro scaling factor of K_i values for transporter inhibition by CsA was conducted by using a previously developed model of rosuvastatin (sensitive index BCRP substrate), and assessing if corresponding DDI ratios were well captured.

Results Within the simulated DDI scenarios for MTX in the presence of CsA, the developed models could capture the observed changes in PK parameters as changes in the area under the curve ratios (area under the curve during DDI/area under the curve control) of 1.30 versus 1.31 observed and the DDI peak plasma concentration ratios (peak plasma concentration during DDI/peak plasma concentration control) of 1.07 versus 1.28 observed. The originally reported in vitro K_i values of CsA were scaled with the uniform qualified scaling factor for their use in the in vivo DDI simulations to correct for the low intracellular unbound fraction of the CsA effector concentration. The resulting predicted versus observed ratios of peak plasma concentration and area under the curve DDI ratios with MTX were 0.82 and 0.99, respectively, indicating adequate model accuracy and choice of a scaling factor to capture the observed DDI.

Conclusions All models have been comprehensively documented and made publicly available as tools to support the drug development and clinical research community and further community-driven model development.

✉ Stephan Schaller
stephan.schaller@esqlabs.com

1 ESQlabs GmbH, Saterland, Germany

2 SGS Exprimo NV, Mechelen, Belgium

3 Galapagos SASU, Romainville, France

4 Simulations Plus, Inc., Lancaster, California, USA

Graphical abstract

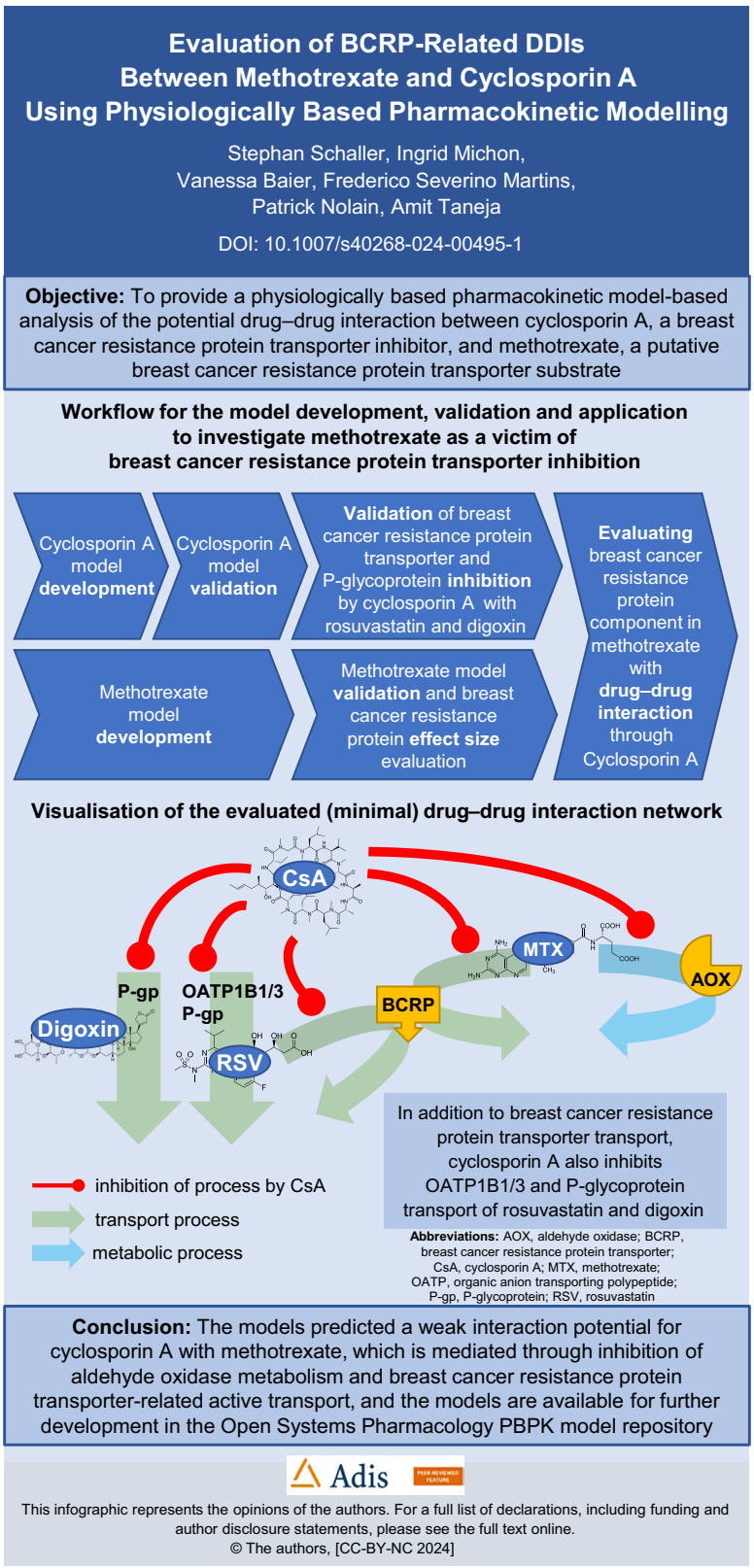

Key Points

Whole-body physiologically based pharmacokinetic (PBPK) models of methotrexate (MTX) and cyclosporin A (CsA) have been developed and evaluated to capture relevant absorption, distribution, metabolism, and excretion-related properties of MTX and CsA to describe the pharmacokinetic (PK) characteristics of MTX and CsA.

These models have been applied to describe and evaluate the CsA-MTX drug–drug interaction (DDI) with the purpose of assessing the effect of breast cancer resistance protein transporter (BCRP) inhibition on MTX PK. To calibrate and cross-qualify the BCRP inhibition by CsA, a published PBPK model for rosuvastatin was used.

The work lays the foundation for the evaluation of DDIs mediated by the BCRP pathway. The models capture a weak interaction potential for CsA with MTX, which is mediated through inhibition of aldehyde oxidase metabolism and BCRP-related active transport, and the models are available for further development in the Open Systems Pharmacology PBPK model repository.

1 Introduction

Characterising drug–drug interactions (DDIs) with drug metabolising enzymes and transporters is a critical part of the drug development process because a drug's exposure following co-administration with another drug can lead to a loss of efficacy or an adverse drug reaction [1]. The DDI risk assessment is initiated at an early stage in drug research by using in vitro tools. Depending on the outcomes of such a risk assessment, clinical DDI studies may be conducted to address the likelihood and potential magnitude of DDIs, and are ultimately used to support labelling requirements and prescribing information [2–4].

The breast cancer resistance protein transporter (BCRP; *ABCG2*) is an ATP-binding cassette efflux transporter that is highly expressed in barrier tissues such as the colon, small intestine, blood–brain barrier, placenta, and liver canalicular membrane and plays a critical role in the oral (PO) absorption and hepatic elimination of substrate drugs [5]. Genetically impaired BCRP activity has been shown to increase exposure to several marketed drugs, including rosuvastatin (RSV), sulfasalazine, and methotrexate (MTX) [6, 7]. While many drugs are inhibitors of BCRP in vitro, there are only a few reported clinically relevant DDIs that are attributed solely to BCRP, in part due to the fact that transporters often have overlapping substrate specificities [8, 9]. For instance, RSV is not only a substrate of BCRP but also of organic anion transporting polypeptides (OATP) 1B1 and 1B3, organic anion transporter OAT3, and P-glycoprotein (P-gp). Transporter-overlapping substrate specificities can often complicate the interpretation of clinical DDI results [10, 11].

Advances in modelling and simulation approaches permit mechanistic and quantitative insights to assist in decision making regarding DDI risk assessments [1]. Physiologically based pharmacokinetic (PBPK) models are mathematical models that mechanistically describe drug pharmacokinetics (PK) based on the physicochemical properties of a drug in combination with the established knowledge on human physiology and by integrating this information within a mechanistic framework [12]. PBPK can thus enable a mechanism-based evaluation of DDI potential [13–15], helping to distinguish the impact of BCRP inhibition on a drug's absorption, distribution, and elimination from effects on other enzymes or transporters, and can be informative for the optimal design of clinical DDI studies.

This study aimed to develop PBPK models of cyclosporin A (CsA; background information in the Electronic Supplementary Material [ESM]), a BCRP inhibitor, and MTX (background info in the ESM), a putative BCRP substrate, to investigate MTX as a victim of BCRP inhibition. With this aim in mind, BCRP transport was incorporated into the MTX model. Metabolism to the primary metabolite 7-OH-MTX by the aldehyde oxidase (AOX) enzyme was included for the stratification of DDI effects, as CsA inhibits both BCRP and AOX, and the model performance was compared with reported PK of MTX and 7-OH-MTX in plasma and urine.

First, we developed a PBPK model of CsA that was able to describe the CsA concentrations in plasma, whole blood, and urine while incorporating relevant absorption, distribution, metabolism, and excretion (ADME) processes to predict intracellular unbound concentrations as effect concentrations of DDIs. Previously developed PBPK models of MTX [16–18] were evaluated but could not be adopted owing to the use of either a different PBPK software or a simpler model structure tailored to and qualified for a different context of use not suitable for DDI evaluations. Similarly, existing PBPK models of CsA were evaluated [19–21]. The model developed by Thiel et al. [20] focused on the cross-species extrapolation of intravenous (IV) data. Jamei et al. [19] developed a CsA model to evaluate DDI with RSV. Both models did not consider the reported binding to cyclophilin (CyP). Zapke et al. [21] developed a model for dose optimisation, extrapolating CyP binding properties from rats. Considering all aspects of the published models and using published clinical data from whole blood, plasma,

and urine, we aimed to develop a refined consensus PBPK model for CsA. The model of CsA as a perpetrator of BCRP inhibition was then qualified using a previously published model of the BCRP-sensitive substrate RSV [22]. The last step in the qualification of the minimal DDI interaction network was the evaluation of the BCRP component in the MTX model by prediction of observed (published) DDIs with CsA.

2 Methods

2.1 Software Used

PBPK models were developed using the open-source modelling software PK-Sim (Open Systems Pharmacology Suite 9.1, www.open-systems-pharmacology.org [23, 24]). Published plasma concentration–time profiles from the literature were digitised with WebPlotDigitizer (www.automeris.io/WebPlotDigitizer). Generation of the goodness-of-fit graphics was done with R (version 1.3.1093; RStudio Inc., Boston, MA, USA).

2.2 PBPK Model Development and Application (Workflow)

For the investigation of MTX as a victim of BCRP inhibition, the developed PBPK models were evaluated and validated prior to their context of use qualification (Fig. 1). PBPK models for both the victim MTX and the perpetrator CsA were first developed and validated using literature PK data and then evaluated for their suitability for capturing DDIs on BCRP using a reference DDI scenario and by investigating the BCRP effect size. The resulting DDI network is depicted in Fig. 1B.

In order to develop the PBPK models for CsA and MTX, a literature search was performed to collect the parameters on physicochemical properties and relevant ADME processes related to the involved drug transporters and metabolising enzymes. The logP, pKa, solubility, and fraction unbound in plasma were obtained using the DrugBank database and literature. In case multiple values were reported in the literature, values for, for example, logP, the fraction unbound in plasma and intestinal permeability, were refined post hoc [14, 20] using the published PK data. The partition coefficients in the tissues were calculated using the method from Rodgers et al. [25]. All CsA-related

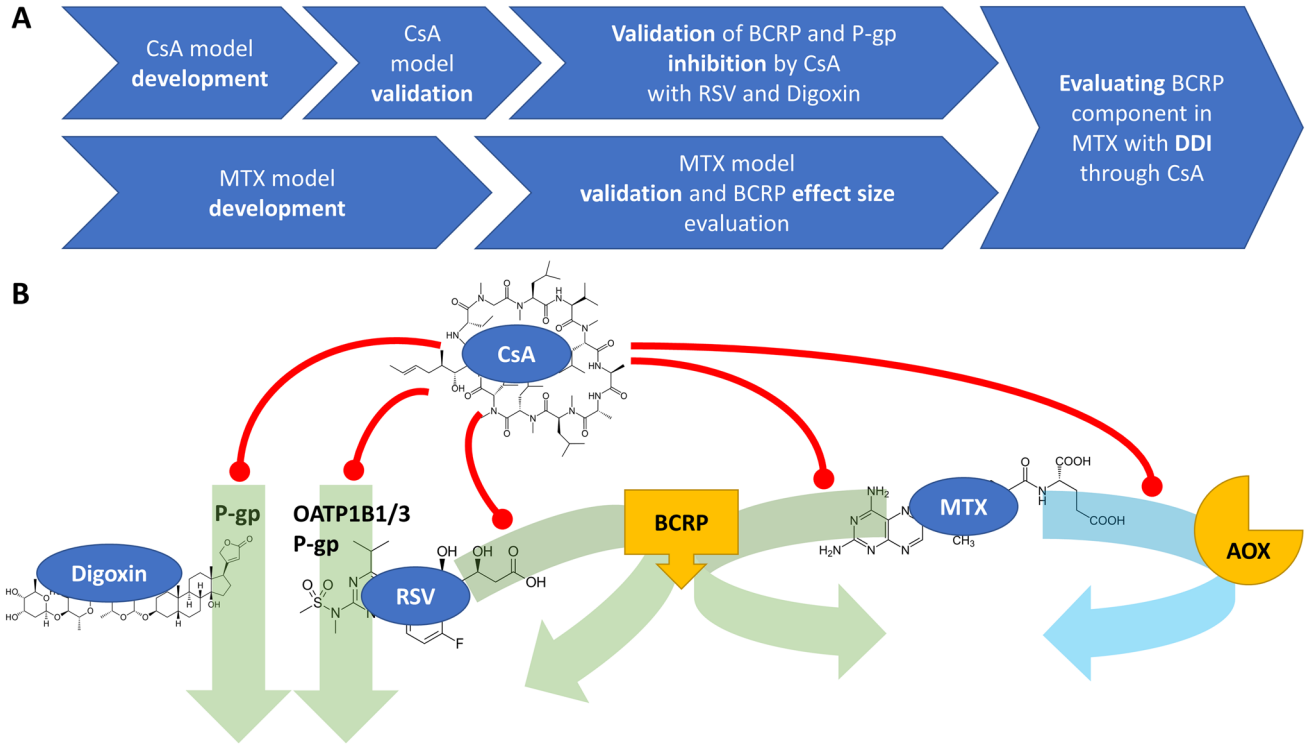

Fig. 1 **A** Workflow for the model development, validation and application to investigate methotrexate (MTX) as a victim of breast cancer resistance protein transporter (BCRP) inhibition. **B** Visualisation of the evaluated (minimal) drug–drug interaction (DDI) network. *Blue arrow* depicts metabolic process, *green arrows* depict transport processes. *Red lines* depict inhibition of processes by cyclosporin A (CsA). In addition to BCRP transport, CsA also inhibits organic anion transporting polypeptides (OATPs) 1B1 and 1B3 and P-glycoprotein (P-gp) transport of rosuvastatin (RSV) and digoxin. *AOX* aldehyde oxidase

and MTX-related, drug-dependent model parameters are listed in Table 1.

To obtain the PK data and PK property/exposure parameters of CsA and MTX, the literature (MEDLINE, PubMed) and the UW DIDB (University of Washington Drug Interaction Database, www.druginteractionsolutions.org) were screened. Primarily studies with known demographic information such as age, sex, height, weight, renal function, dosing information, available plasma concentration–time profiles and/or exposure parameters were included in the model development. The studies used for model development for MTX and CsA are listed in Tables S1 and S2 of the ESM. Further background on the PBPK model structure is outlined in Sect. 3 of the ESM. Criteria for the model goodness-of-fit evaluation are outlined in Sect. 2.6.

2.3 PBPK Model of CsA

The PBPK model for CsA was built by incorporating all physicochemical compound-related properties as outlined in Sect. 2.1, Table 1, and was subsequently refined using the observed clinical data extracted from the literature (Table S2 of the ESM) with different formulations (Neoral Soft Gelatin Capsules, Sandimmune Soft Gelatin Capsules and Oral Solution, Novartis). Cyclophilin binding was incorporated into the model using the PK-Sim tissue expression and a protein binding kinetic, while the observed rapid red blood cell uptake was accounted for by incorporating an increased permeability into red blood cells (0.1 cm/min; scaled by 10e4 from 1×10e-5 cm/min). Higher than predicted permeability was also incorporated in the tissue extravasation kinetics by an increased cellular permeability (P [interstitial →

Table 1 Cyclosporin A and methotrexate drug-dependent model parameters

Parameter	Unit	Cyclosporin A		Methotrexate	
		Value (origin)	Source (origin)	Value (origin)	Source (origin)
MW	g/mol	1202.6	–	454.4	–
pKa basic	–	n.a.	DrugBank	5.5	DrugBank
pKa acid	–	11.83	DrugBank	4.8	DrugBank
LogP	–	3 (1.9–3.4)	Refined ([45, 54, 55])	−1.85	DrugBank (exp. LogP)
Solubility	mg/L	1.5 (0.0093)	Fitted ([56])	3000	Bolger et al. (poster, measured FaSSIF)
Intestinal permeability	10e-6 cm/min	1200 (2.75)	Fitted ([57])	60	[26] Table 3
B:P ratio	–	1.24 (0.2–4)	Predicted ([45, 55, 58])	0.55	Predicted
$f_{u(human)}$	%	12 (3.5–17)	Refined ([45, 55, 59])	40 (42–57)	Refined ([59])
CYP3A4 V_{max}	pmol/min/pmol	5 (0.024–5)	Refined ([58, 60, 61])	–	–
CYP3A4 Km	µmol/L	1.7 (1.2–2.2)	Refined ([60])	–	–
AOX V_{max}	µmol/min/L	–	–	3.41	Fitted
AOX Km	µmol/L	–	–	2792	[62]
AOX reference concentration	µmol/L	–	–	2.5	Fitted
P-gp V_{max}	pmol/min/pmol	10 (–)	Fitted ([63])	–	–
P-gp Km	µmol/L	6.1 (3.8–8.4)	Refined ([63])	–	–
BCRP V_{max}	µmol/L/min	–	–	3982 (2500)	Fitted [64]
BCRP Km	µmol/L	–	–	1340	[65]
AOX K_i	nmol/L	2	Fitted	–	–
BCRP K_i	µmol/L	0.05 (0.25–7.2)	Fitted ([66])	–	–
P-gp K_i	µmol/L	0.04 (0.9–3.2)	Fitted ([67])	–	–
OATP1B3 K_i	µmol/L	0.007 (0.03–2.2)	Fitted ([38, 66, 68])	–	–
OATP1B1 K_i	µmol/L	0.007 (0.03–2.2)	Fitted ([38, 66, 68])		
GFR fraction	–	–	–	1.0	[69]
Renal CL (plasma)	L/h/kg	–	–	0.0085	[69] Tubular Secretion

"Refined" indicates that the values have been identified by parameter identification to a value within ranges of values found in the literature. Original ("origin") literature values are provided in brackets. "Fitted" indicates that these values have either not been reported, or the obtained values resulting from the fit are outside the range of the values found in the literature. "Predicted" values are calculated using PK-Sim-intrinsic methods based on compound properties

AOX aldehyde oxidase, *BCRP* breast cancer resistance protein transporter, *B:P* blood plasma ratio, *CL* clearance, f_u fraction unbound in plasma, *GFR* glomerular filtration rate, *MW* molecular weight, *n.a.* not applicable, *OATP* organic anion transporter peptide, *P-gp* P-glycoprotein

intracellular] increased seven-fold for non-mucosal tissue), based on experimental PK data used for fitting (Table S2 of the ESM). Elimination of CsA was implemented as metabolism through cytochrome P450 (CYP) 3A4 (Michaelis–Menten kinetics), forming metabolites (M1 + M17), and CsA is excreted unchanged to urine at relatively low rates through P-gp.

2.4 PBPK Model of MTX

The PBPK model for MTX was built by incorporating physicochemical and compound-related properties as outlined in Sect. 2.1, Table 1, and subsequently refined using the observed clinical data extracted from the literature (Table S1 of the ESM see ESM Sect. 3 and Figs. S1 and S2 for details on model structure). MTX is classified as class III as per the Biopharmaceutical Classification System (high solubility and low permeability) [26]. For the developed PBPK model, three different formulations were used, differing in time to 50% dissolution (30, 60, and 90 minutes, Weibull dissolution function), and calibrated based on PO PK. MTX is a substrate of BCRP (included in the model as Michaelis–Menten kinetics) and is also a substrate for active transport by OAT1 and OAT3, and multidrug resistance-associated protein 2 and multidrug resistance-associated protein 4 (the latter transporters were not included in the model because of a lack of required data) [27]. In addition, MTX is considered to be a substrate of OATP1Bs [28, 29], but conclusions on the pharmacogenomic impact of the OATP1B polymorphism remain controversial [30]. However, clinical DDIs of CsA on MTX through OATP1B have not been studied specifically or mentioned as a relevant interaction pathway [31]. Consequently, OATP1Bs have not been included in the model. The initially predicted cellular uptake based on compound lipophilicity and molecular weight underpredicted the volume of distribution of MTX, i.e. tissue partitioning, and model refinement suggested a 50-fold increased cellular permeability (interstitial → intracellular) compared with experimental PK data. Thus, the higher than initially predicted tissue uptake could be attributed to the omission of the aforesaid additional drug transporters. Elimination of MTX was implemented as metabolism through AOX, forming a metabolite (7-OH-MTX) using Michaelis–Menten kinetics, and excreted unchanged into urine through glomerular filtration and active tubular secretion.

2.5 Virtual Individual Characteristics

For virtual individuals and populations used in the simulations, the "European Standard Male" (default settings for male using the "European [ICRP, 2002]" population in PK-Sim [32]) was used as a basis. The population used for the MTX model was defined as an adult population of mixed sex ($n = 100$, aged 18–65 years, 50% female).

For enzyme and transporter expressions, the original database entries (OSP Expression Database for OSP version 9.1), modified as outlined in the respective publications, were used as follows: P-gp and BCRP: OSP-wide aligned P-gp expression as used by Hanke et al. [22]; CYP3A4: OSP-wide aligned CYP3A4 expression as used by Frechen et al. [33]; AOX: original "RT-PCR" entry; and CyP: original "EST" entry. "OSP-wide aligned" in this context means the modified (from the original database entry) expression used in the qualified template models of the respective OSP version (version 9.1).

2.6 Model Evaluation and Sensitivity Analysis

The PBPK model goodness-of-fit criteria have been evaluated based on the PK properties C_{max} (peak plasma concentration) and AUC_{last} (area under the curve from the first until the last measured point) and compared with observed data (Equations S1 and S2 with the mean fold error and its geometric mean fold error in the ESM; and goodness-of-fit plots in Sect. 3.1 CsA PBPK model building and evaluation, and Figs. 4 and 7).

Model sensitivity across parameters has been evaluated to investigate the impact of parameter uncertainty on the model simulation outcomes. A parameter sensitivity analysis was conducted in PK-Sim (ESM "Sensitivity Analysis" Section and Figs. S4 and S5 of the ESM for CsA, and Figs. S6 and S7 of the ESM for MTX).

2.7 DDI Model Network Development, Qualification, and Evaluation

The DDI model network for the evaluation of BCRP-related DDIs was built using two victim compounds, MTX and RSV, and the perpetrator compound CsA. The models for MTX and CsA were developed de novo as outlined above, while the originally published and qualified model for RSV [22] was used for this analysis to evaluate the CsA DDI properties, including its effect on BCRP. The performance of the DDI simulations was assessed by comparing predicted and observed plasma time–concentration profiles of the victim drug, administered alone and with perpetrator co-administration (Tables 2 and 3).

CsA inhibits both BCRP and AOX. While no K_i values are known for AOX, multiple K_i values for the inhibition of BCRP by CsA have been reported in the literature (7.8 µmol/L [34] and 0.25–0.75 µmol/L [35, 36]). CsA is reported to affect the kinetics of MTX with increasing area under the curve (AUC) by a factor of 1.31 [31], caused by the inhibition of BCRP and AOX. The K_i listed in Table 1

Table 2 Comparative DDI evaluation between literature data and PBPK simulation outcomes for RSV dosed with CsA [38]

Dose CsA	Dose RSV	$AUCR_{obs}$	$AUCR_{pred}$	$C_{max}R_{obs}$	$C_{max}R_{pred}$	$AUCR_{pred/obs}$	$C_{max}R_{pred/obs}$
200 mg BID	10 mg SD	5.50	5.07	9.11	10.81	0.92	1.19
200 mg BID	20 mg SD	8.02	9.54	15.18	18.38	1.19	1.21

For control, only data from RSV 10-mg dosing were available, and the ratios for the RSV 20-mg DDI scenario were also calculated against the RSV 10-mg baseline. $C_{max}R_{pred}$ or $AUCR_{obs}$: ratio in C_{max} or AUC of observed or predicted data with and without dosing of CsA

AUC area under the curve, *AUCR* area under the curve ratio, *BID* twice daily, C_{max} peak plasma concentration, $C_{max}R$ ratio of peak plasma concentration, *CsA* cyclosporin A, *DDI* drug–drug interaction, *obs* observed, *PBPK* physiologically based pharmacokinetic, *pred* predicted, *RSV* rosuvastatin, *SD* single dose

Table 3 Comparative DDI evaluation between literature data and PBPK simulation outcomes for MTX dosed with CsA [31] with varying K_i values for CsA inhibition of BCRP transport

K_i value	$AUCR_{obs}$	$AUCR_{pred}$	$C_{max}R_{obs}$	$C_{max}R_{pred}$	$AUCR_{pred/obs}$	$C_{max}R_{pred/obs}$
7.8 µmol/L	1.31	1.02	1.28	1.02	0.78	0.79
0.25 µmol/L	1.31	1.15	1.28	1.04	0.87	0.82
0.05 µmol/L	1.31	1.30	1.28	1.05	0.99	0.82

CsA was dosed with 1.5 mg/kg BID and MTX with a single 15-mg dose. $AUCR_{obs}$ or $C_{max}R_{pred}$: ratio in AUC or C_{max} of observed or predicted data with and without dosing of CsA

AUC area under the curve, *AUCR* area under the curve ratio, *BCRP* breast cancer resistance protein transporter, *BID* twice daily, C_{max} peak plasma concentration, *CsA* cyclosporin A, *DDI* drug–drug interaction, *MTX* methotrexate, *obs* observed, *PBPK* physiologically based pharmacokinetic, *pred* predicted

were used in the model to predict the reversible inhibitory potential of CsA as a competitive inhibitor of BCRP.

For the DDI predictions, simulations using study-representative individuals were conducted to quantify the DDI impact caused by CsA through changes in plasma concentrations, i.e. C_{max} and AUC_{last} ratios, for single PO doses, as reported in studies from the literature (Tables 2 and 3).

3 Results

3.1 CsA PBPK Model Building and Evaluation

Twelve clinical studies with IV or PO administration of CsA were used (Table S2 of the ESM) in the model development ($n = 4$) and validation ($n = 8$) processes, with doses that range from 2 to 1400 mg in single-dose regimens. All simulations were based on the relevant ADME properties and were set up according to study protocols as described in the respective publications.

The PK after IV dosing were evaluated using both plasma and whole blood concentration–time profiles. Because of the non-linearity in the blood/plasma partitioning of CsA, the PK curve shapes of these two sampling matrices significantly differ between studies depending on the dose and resulting exposure levels. Whole blood PK show a faster increase but lower C_{max} (saturates at lower concentrations), and plasma PK show a slower initial increase and reach higher C_{max} levels but are subject to a faster distribution, i.e. a faster decline after reaching C_{max}.

Results after IV infusions (all IV studies) are shown in Fig. 2 (Panels A, B, and I) for whole blood (and plasma in Fig. 2, Panel A) concentration–time profiles. Results after PO dosing are shown in Fig. 2 (Panels C–H) for whole blood (and plasma in Fig. 2, Panel C) concentration–time profiles.

For quantification of CsA metabolism, the total concentrations of the CsA metabolites M1 + M17 were included in the simulations where observed data were available (Fig. 3). Good agreement between simulations and data was achieved. Nevertheless, metabolite PK showed an early onset of metabolite appearance after CsA dosing, which was not captured by the model (also for tested lower [high affinity] K_m values for faster CsA metabolism at lower concentrations). Overall, all studies except one (1400 mg from Reymond et al. [37]; AUC ratio [AUCR] = 0.43) were described by the PBPK model within two-fold of the corresponding observed values (e.g. mean fold error 0.5–2.0). The quantitative comparisons of predicted and observed PK parameters of CsA are shown in Fig. 4.

3.2 Qualification of CsA as an Inhibitor of BCRP-Related Drug Transport with BCRP Substrate RSV

The qualification for a BCRP-related DDI with RSV as a substrate and CsA as an inhibitor is based on publicly

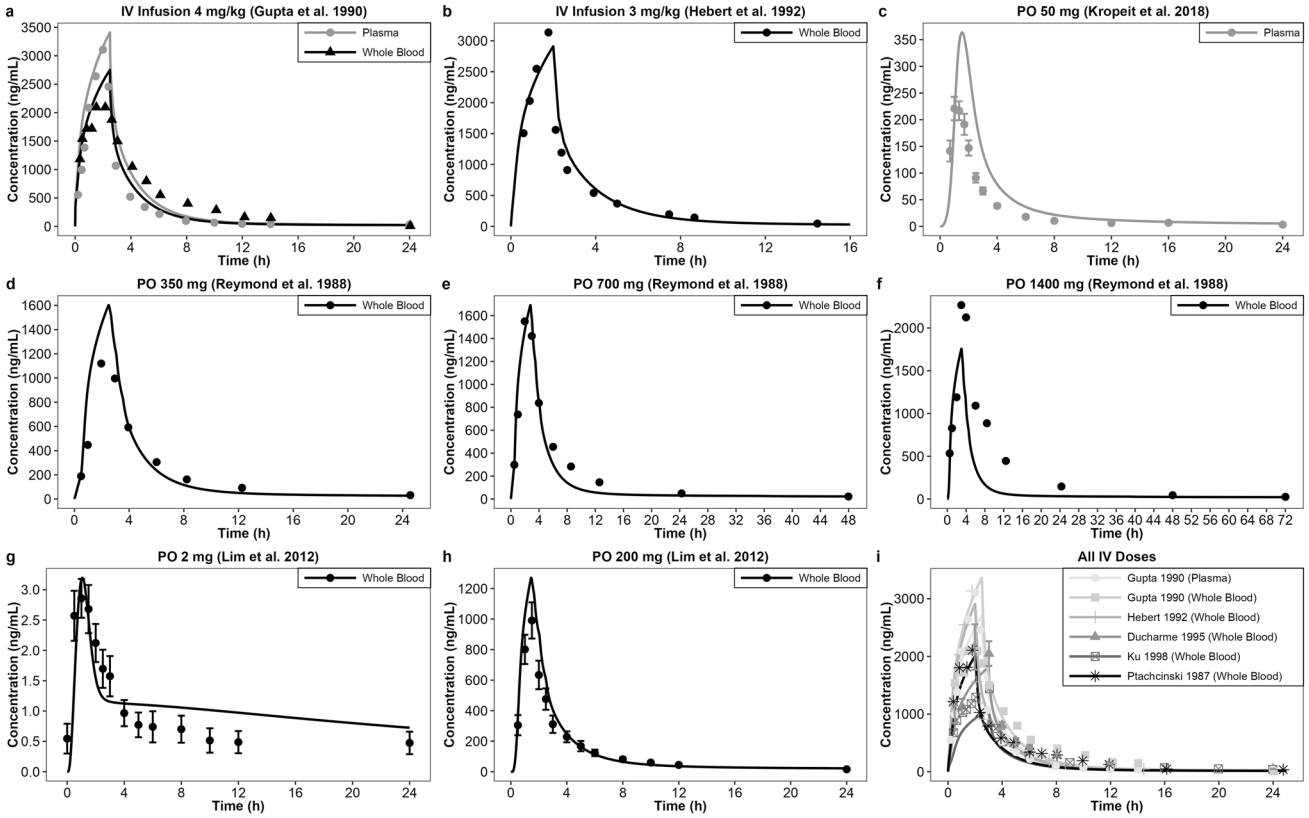

Fig. 2 Observed and predicted whole blood (and plasma, panel **a** and **b**) pharmacokinetic profiles of cyclosporin A (CsA) in peripheral venous blood following single intravenous (IV) and oral (PO) doses that range from 2 to 1400 mg (linear scale). *Symbols* represent the observed, and *lines* represent the simulated time–concentration profiles of CsA. Formulations used are: Sandimmune Capsule (panels **c–f**) and Neoral (panels **g** and **h**). Panel **i** shows all IV data. Observed data are referenced in Table S2 of the ESM. *h* hours

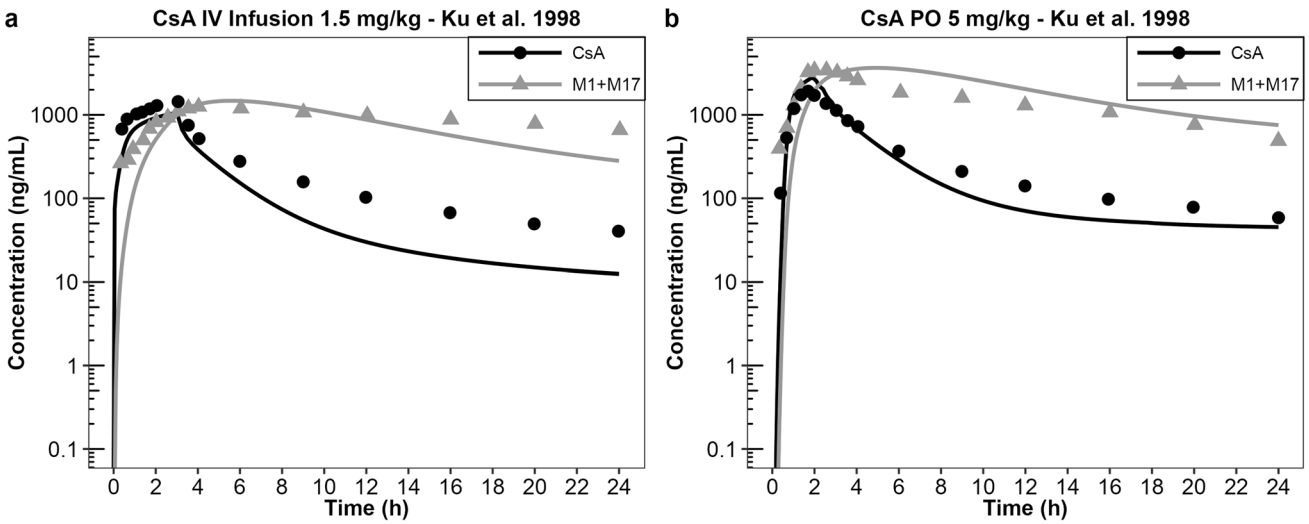

Fig. 3 Observed (*symbols*) and predicted (*lines*) whole blood pharmacokinetic profiles of cyclosporin A (CsA) [*black*] and metabolites M1 + M17 (*grey*) following a 1.5-mg/kg intravenous (IV) dose (panel **a**) and a 5-mg/kg oral (PO) dose (panel **b**) of CsA. Plots are on a log scale. Observed data are referenced in Table S2 of the ESM. *h* hours

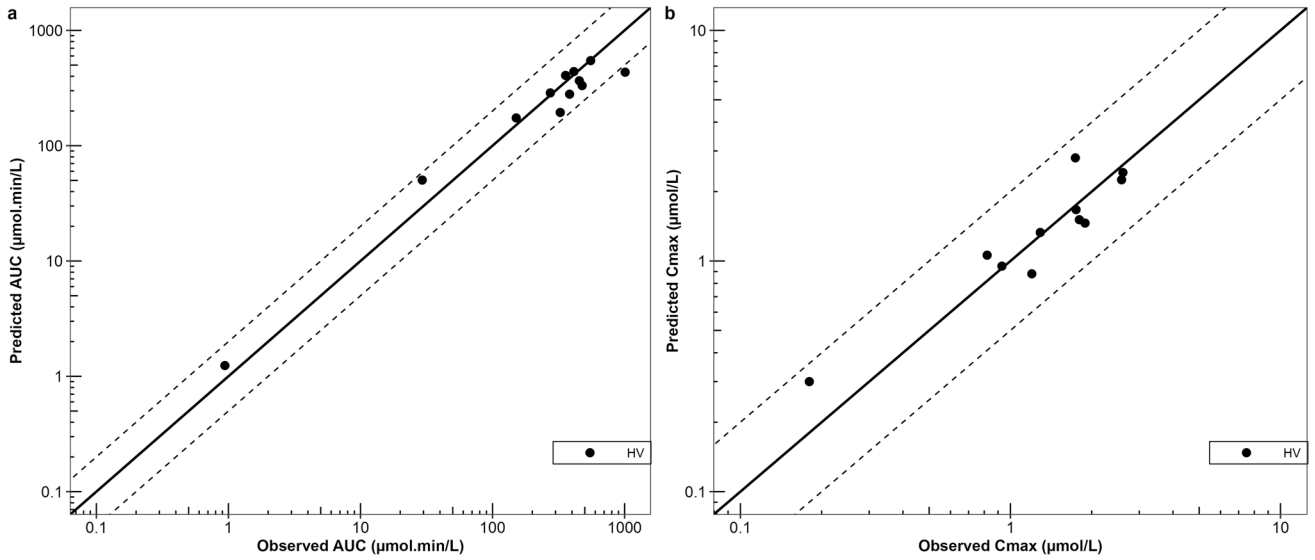

Fig. 4 Comparison between simulated and observed pharmacokinetic parameters of cyclosporin A from all studies. *Solid lines* represent the line of unity; *dashed lines* represent a two-fold difference. *AUC* area under the curve, C_{max} peak plasma concentration, *HV* healthy volunteer

available data [38]. The outcomes from clinical DDI studies are shown in Fig. 5 and summarised in Table 2.

During the DDI study, subjects received either CsA 200 mg twice daily (continuous treatment) or placebo and were given a single PO dose of either 10 or 20 mg of RSV. The in vitro K_i for CsA-affected processes (BCRP and OATP1-B1 and OATP1-B3 and P-gp transport) were scaled uniformly across all pathways, and not per individual pathway, throughout all DDI evaluations with CsA and reduced globally to align with the MTX-CsA DDI scenario by a factor of approximately 50 to account for differences between in vitro and in vivo conditions, i.e. the unbound intracellular concentrations of CsA in vivo (exact factor depends on the selected reference K_i from the literature, e.g. for BCRP, reported K_i values range from 0.25 to 7.8 µmol/L [34, 35]; the 50-fold reference would correspond to an in vitro K_i value of 2.5 µmol/L). Simulated/observed ratios for the C_{max} ratio and AUCR of RSV were within 1.25-fold, confirming that the effect of CsA on RSV could be predicted accurately (Table 2).

3.3 Cross-Validation of the Empirical Uniform Scaling Factor for CsA K_i Values

Given the non-specificity of RSV as a substrate for the CsA-affected transport processes (BCRP and OATP1-B1 and OATP1-B3 and P-gp transport), a consistent scaling of the IVIVE for the K_i values across transporters and substrates for CsA is key. Notably, the BCRP effect size in the RSV PBPK model is low (AUCR of a BCRP knock-out of approximately 1.15, depending on the simulated scenario) as compared with both the P-gp effect size (AUCR of a P-gp knock-out of >5) and genetic variation (single nucleotide polymorphism) effect size (AUCR ranges between 2-fold and 2.5-fold); however, there are uncertainties in these data [7]. Thus, the empirical uniform scaling of the K_i values utilised in the CsA DDI assessment with RSV was further assessed with the P-gp substrate digoxin [39]. In the study from Dorian et al. [40], indirect PK-related metrics of DDI effects, such as a change in clearance, were reported. In this study, a digoxin PO dose of 1 mg was administered to patients with and without concomitant PO dosing with CsA 200 mg. While the study did not report changes in AUC or C_{max}, a change in the apparent volume of distribution of digoxin (decreased by 71%) and its plasma clearance (decreased by 53%) was reported [40]. For the simulation of the reported DDI scenario, the model predicted an increase in both AUC and C_{max} by 45%, which is in line with the reported changes in volume of distribution and plasma clearance, confirming the empirical uniform scaling factor for CsA K_i values.

3.4 MTX PBPK Model Building and Evaluation

A total of 26 clinical studies with IV or PO administration of MTX were used (Table S1 of the ESM) for model development, i.e. training ($n = 9$) and validation ($n = 17$), with doses that ranged from 2.5 to 20 mg in single-dose or multiple-dose regimens. Individual PBPK model simulations of MTX have been set up according to each study protocol, which incorporate relevant ADME properties. Representative results for IV and PO dosing are shown in Fig. 6; further

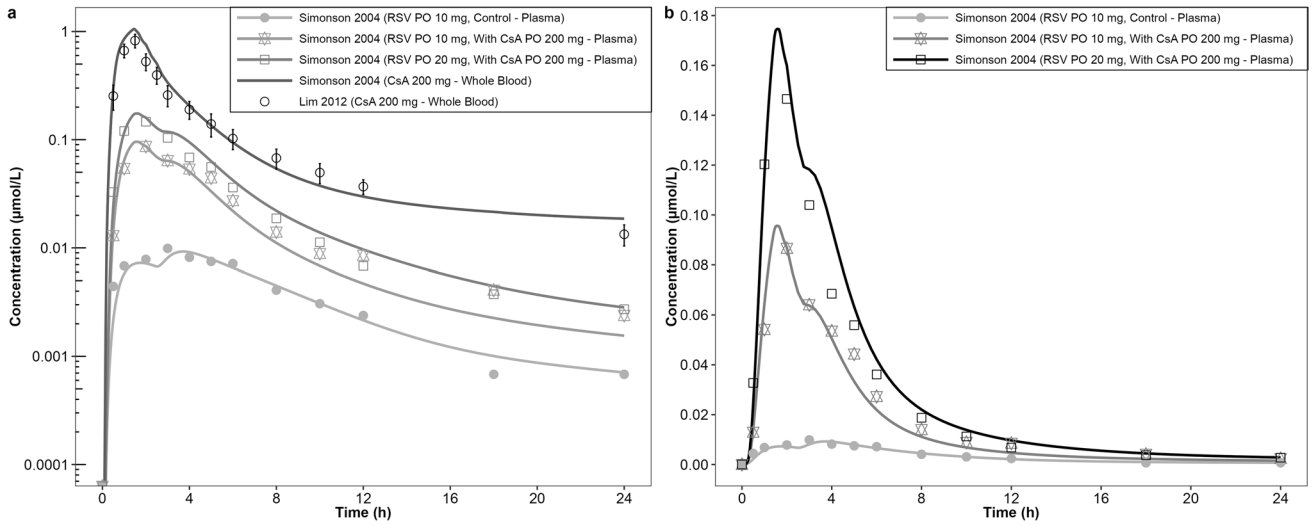

Fig. 5 Qualification of cyclosporin A (CsA) as an inhibitor of breast cancer resistance protein transporter (BCRP)-related drug transport with BCRP substrate rosuvastatin (RSV), displaying concentration–time curves for RSV (and CsA) pharmacokinetics (PK) with and without co-administration of CsA. Patients received 10 g of RSV alone (control; no data are available for the 20-mg control cohort) or 10 mg or 20 mg of RSV with 200 mg of CsA [38]. The *left panel* is on a log scale and includes CsA PK that were not reported with the study, but observed data were taken from Lim et al. [70] (see also Fig. 2, panel **h**), which were omitted from the *right panel* for improved visualisation. *h* hours, *PO* orally

results across dose ranges are shown in Figs. S9 and S10 of the ESM.

For the two studies shown in Fig. 6, the model predicted versus observed C_{max} and AUC_{last} ratios were, respectively, 0.74 and 0.64 for IV dosing and 1.1 and 1 for PO dosing. Overall, predicted versus observed C_{max} and AUC_{last} ratios were in the range of 0.51–1.6 and 0.51–1.82, respectively, with a single outlier of 3 for both C_{max} and AUC. The quantitative comparisons of predicted and observed PK parameters of MTX are shown in Fig. 7. For the metabolite 7-OH-MTX, these are shown in Fig. S3 of the ESM. For the MTX PK C_{max} and AUC_{last} ratios, a geometric mean fold error (C_{max}) = 1.00 and geometric mean fold error (AUC_{last}) = 0.98 was achieved.

The population simulation-based evaluation was conducted for 7.5-mg and 15-mg single-dose studies for which the most data were available (Fig. 8). The population simulation demonstrates a good agreement of the 5th–95th percentile range of simulated time–concentration profiles with the observed data. It has to be noted that the simulated population (n = 100, 50% female, aged 18–65 years) corresponds to a mean healthy population and does not represent all study populations used in the figure. Pathophysiological changes in patient populations and fixed dosing regimens instead of bodyweight-based dosing do not allow for a direct quantitative comparison. Additional simulation results for MTX can be found in Figs. S9 and S10 of the ESM.

3.5 Evaluation of DDI of CsA with MTX

For the evaluation of the DDI between MTX and CsA, the only published scenario from Fox et al. [31] was used (summary in Table 3). The reported C_{max} and AUC were 1.28 and 1.31, respectively. For CsA inhibition of BCRP transport, the PBPK model predicted an AUCR of 1.02 and 1.14 using the BCRP K_i values 7.8 and 0.25 µmol/L, respectively, obtained from the literature [34, 35].

In light of this underprediction of the DDI effect, an evaluation of the total effect size of BCRP transport on MTX PK, a BCRP "knock-out" scenario was simulated to investigate if the model would be able to capture the DDI effect for lower K_i values at all. A pharmacogenomic analysis of several single-nucleotide polymorphisms in BCRP by Liu et al. [41] showed a maximal reduction of 16% of total clearance after IV dosing. Switching off BCRP in the model results in a reduction in total body CL of 45% after either IV or PO dosing, and an 8% increase in C_{max} and a 71% increase in AUC (see also Fig. S8 of the ESM). This indicated a sufficient maximum effect size of BCRP in the model to capture the outcome of the reported DDI [31], which was reported as a 28% and 31% increase in C_{max} and AUC, respectively (within 1.5-fold). A second consideration is a reduced sensitivity to the efflux transporter due to high bioavailability (F) and intestinal availability (FaFg). Bioavailability was calculated to be 95% with an Fa of 1. These values result from literature-reported values on the solubility and intestinal permeability. Given the sufficient BCRP effect size and the

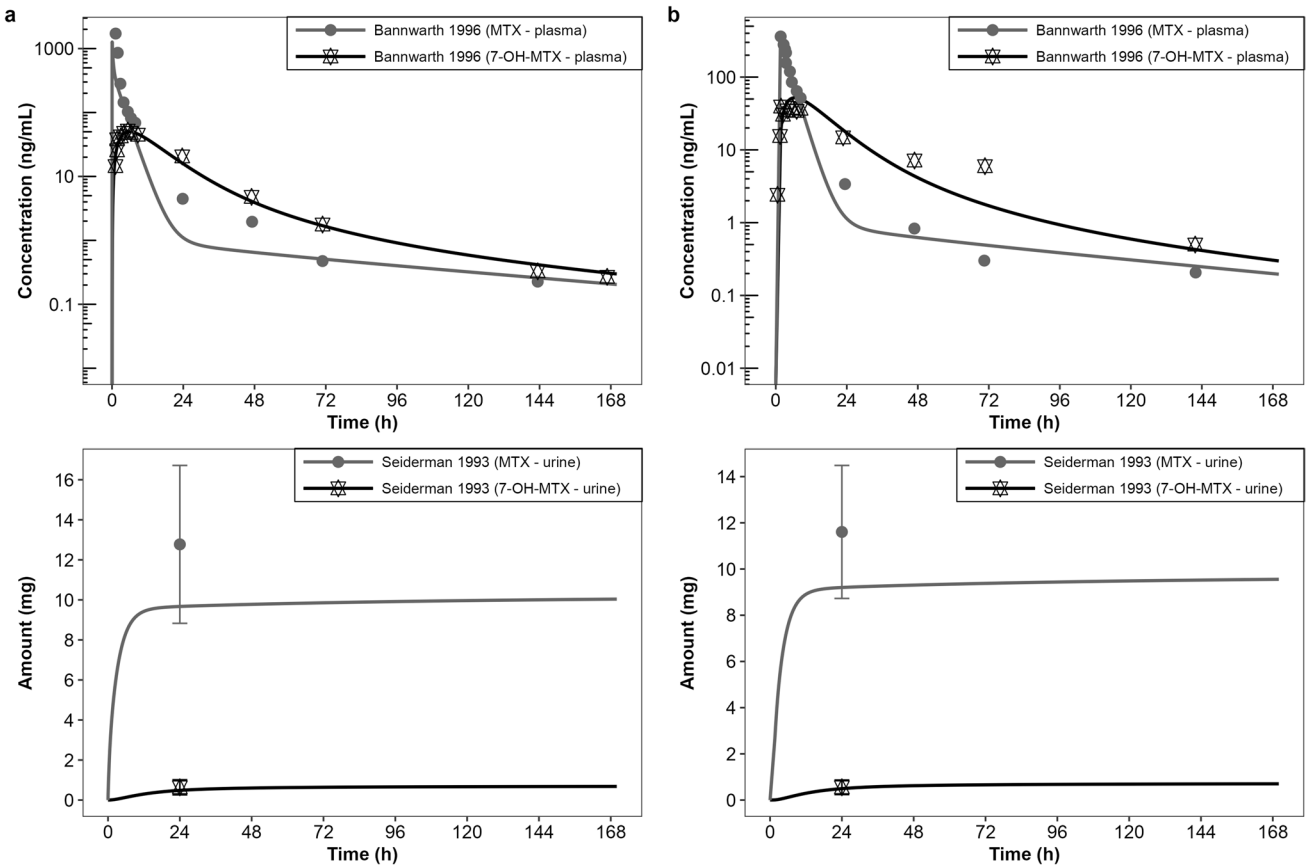

Fig. 6 Outcomes for the methotrexate (MTX) PBPK model development using training data sets (Table S1 of the ESM) for doses of 15 mg intravenously (*left panel*) and orally (*right panel*). *Grey dots and curves* represent observed and simulated data for MTX, while *black stars and curves* represent observed and simulated data for MTX metabolite 7-OH-MTX. *Top panels* correspond to the plasma concentration–time curves, while *bottom panels* depict the amount of the respective compounds excreted in urine over time. Plots are on a log scale. *h* hours, *PBPK* physiologically based pharmacokinetic

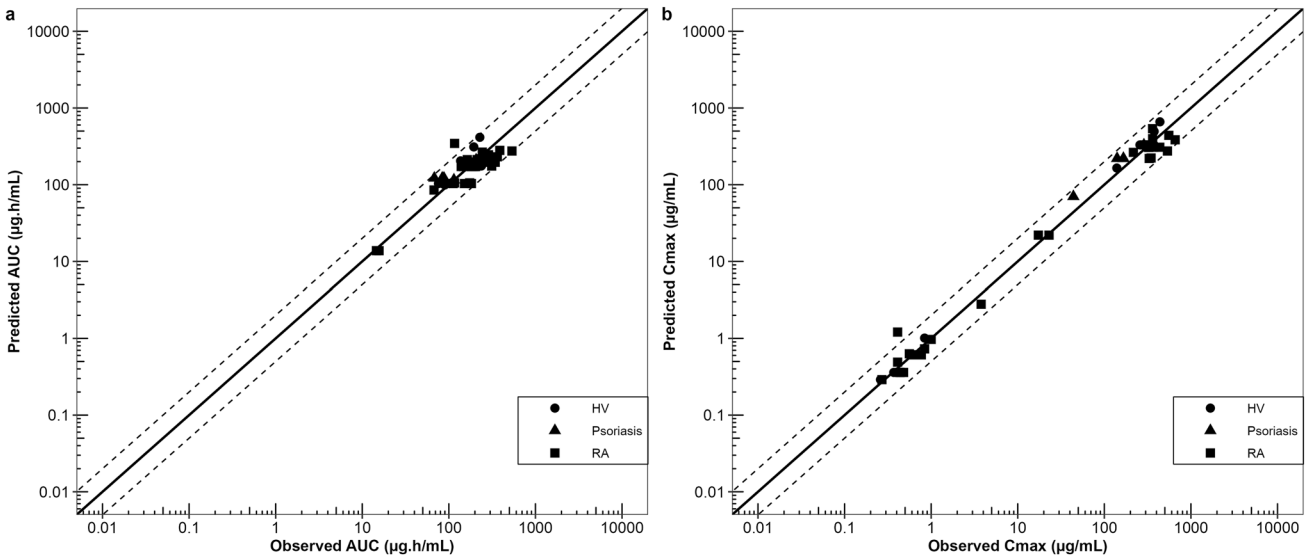

Fig. 7 Comparison between simulated and observed pharmacokinetic parameters area under the curve (AUC) [*left panel*] and peak plasma concentration (C_{max}) [*right panel*] of methotrexate from all studies, separated by population types. *Solid lines* represent the line of unity; *dashed lines* represent a two-fold difference. *HV* healthy volunteer, *RA* rheumatoid arthritis

good model performance capturing the PK after PO application, a further adjustment of parameters related to intestinal passive uptake was not deemed necessary.

Based on the observed data, the K_i of CsA on BCRP was thus reduced to 0.05 µmol/L by model fit, scaled to account for differences between in vitro and in vivo conditions, i.e. the unbound intracellular concentrations of CsA in vivo. Published in vitro K_i values have been reported in the range of 0.25–7.8 µmol/L [34, 35]. The scaling factor was consistent with the scaling of the K_i values in the CsA–RSV DDI in Sect. 3.2 and the CsA–Digoxin DDI in Sect. 3.3.

Using the scaled BCRP K_i of 0.05 µmol/L, the simulated AUCR increased to 1.30, which is very similar to the observed value of 1.31 (Table 3). While an increase in AUC of about 30% is almost non-significant, based on the 80–125% equivalence thresholds, the data also reflect the effect on a qualitative level. The characteristic observed increase in intestinal uptake and decrease in renal excretion, due to inhibition of intestinal BCRP, in combination with the reduction of MTX metabolism, due to inhibition of AOX, resulted in both the slight increase of C_{max} and a delay of T_{max} for MTX, and was captured by the model (Fig. 9, upper panels). Also, the reduction in urinary excretion through the inhibition of the efflux transporter BCRP, as reflected by the increase in AUC and decrease in renal excretion, is well captured (Fig. 9, lower panels), as is the effect on the metabolite formation through AOX and its reduced excretion to urine (K_i of CsA for AOX was fitted).

4 Discussion

For this study, PBPK models of CsA, an established inhibitor of BCRP, and MTX, a putative BCRP substrate, were developed to assess the effect of BCRP inhibition on MTX PK. Both the PK of CsA and MTX were adequately captured by the developed PBPK models. CsA was validated by evaluating CsA as a perpetrator of BCRP inhibition using

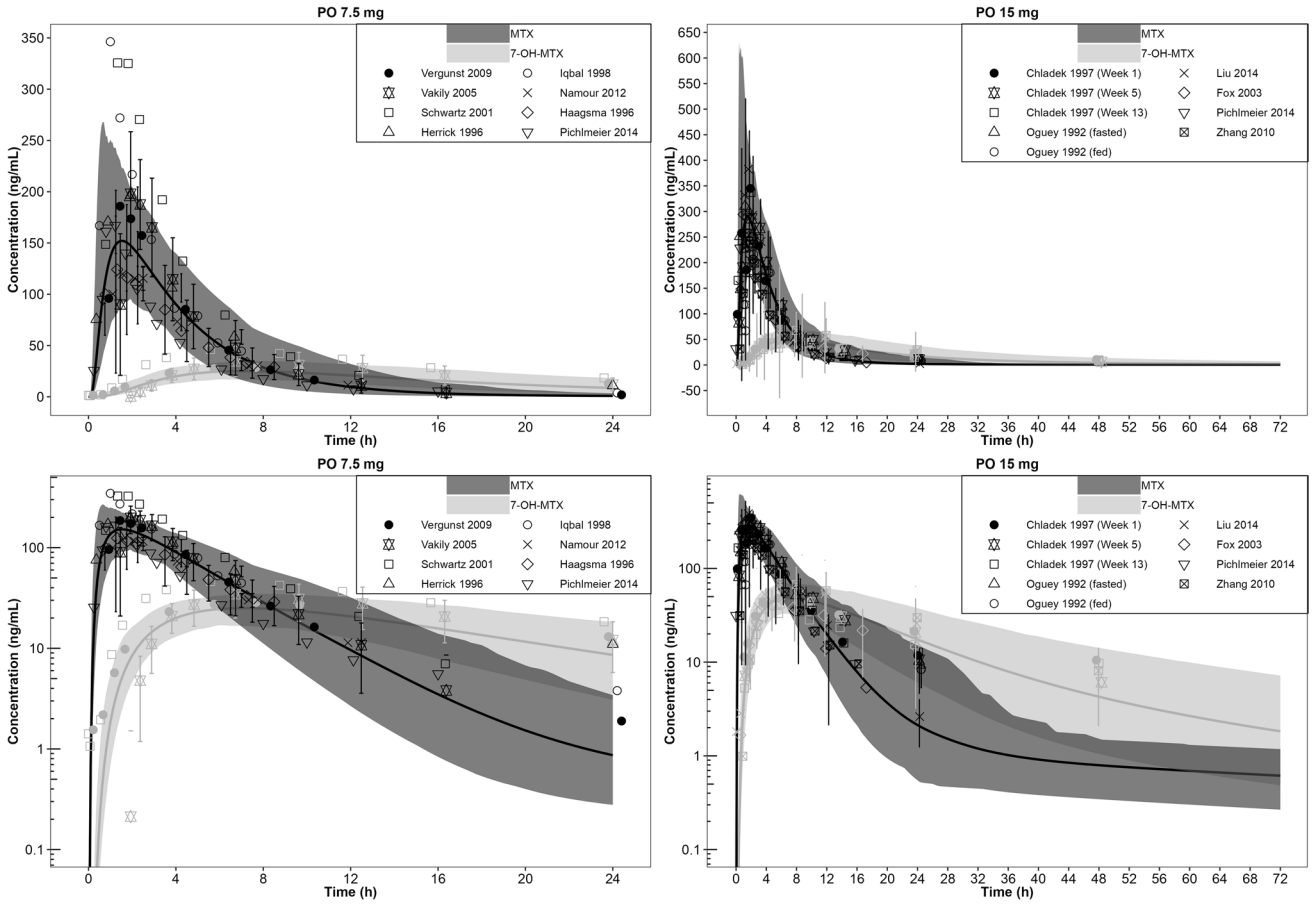

Fig. 8 Methotrexate (MTX) PBPK model qualification using validation data sets (Table S1 of the ESM) for oral (PO) doses of 7.5 and 15 mg. *Black dots and curves* represent observed and simulated data for MTX, while *grey dots and curves* represent observed and simulated data for MTX metabolite 7-OH-MTX. The *shaded areas* correspond to the 5th–95th percentile range of simulated time–concentration profiles of a population simulation (n = 100, 50% female, aged 18–65 years). Plots are on a log scale. *h* hours, *PBPK* physiologically based pharmacokinetic

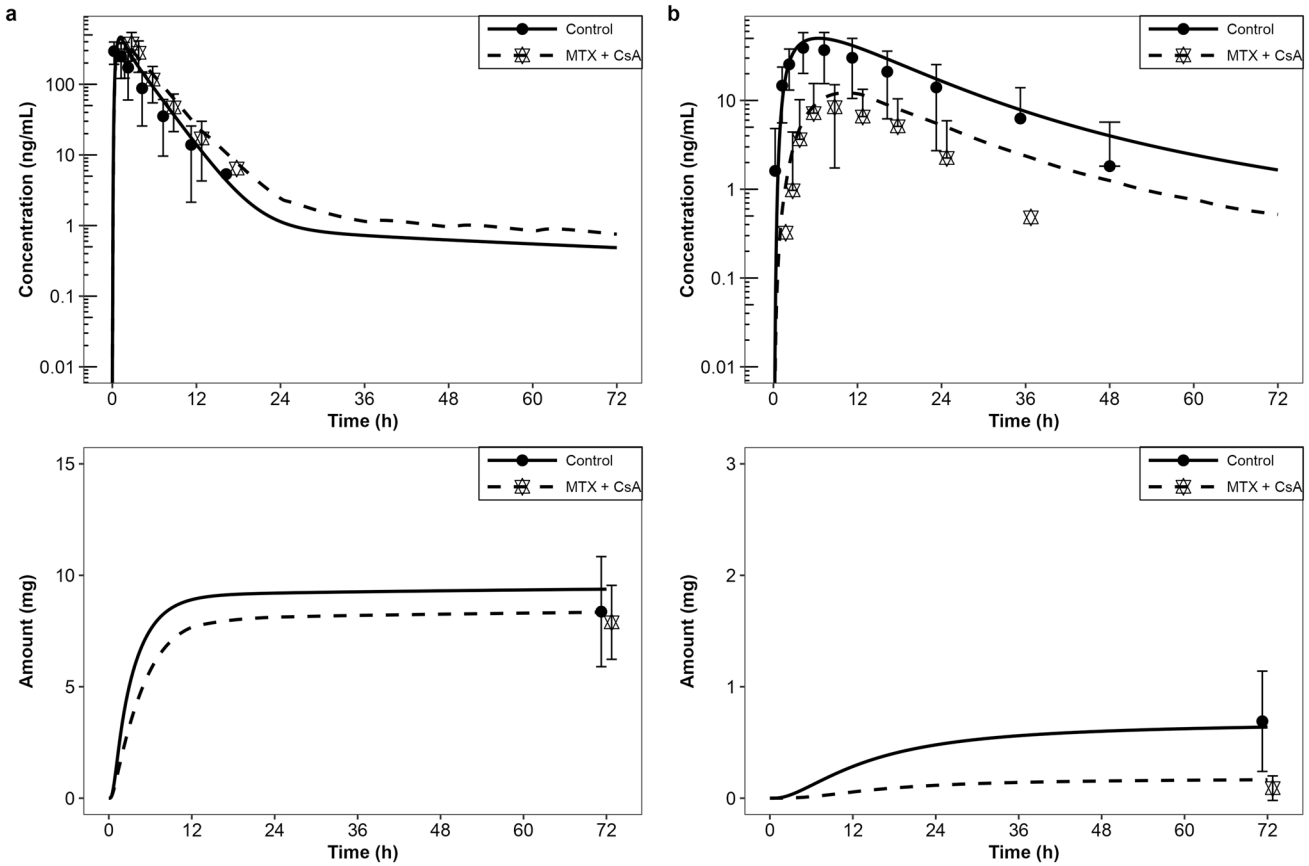

Fig. 9 Single oral dose of methotrexate (MTX) 15 mg combined with oral doses of cyclosporin A (CsA) 1.5 mg/kg twice daily. *Left panels* represent plasma concentrations (*top*) and the amount excreted in urine (*bottom*) for MTX and *right panels* represent the same for MTX-OH. *Solid lines and dots* represent the control arm, whereas *dashed lines and stars* represent the arm with concomitant treatment with CsA. *h* hours

RSV, a known BCRP substrate, as the victim drug [42]. The K_i values for CsA DDI were uniformly scaled by a factor of 50. This scaling is meant as a correction of the unbound fraction in the IVIVE translation of the K_i values utilised. The original parameterisation of transporters in the model (and the corresponding fraction of contribution) as well as the original relative difference for all CsA in vitro K_i values was retained. Refining the models with transporter-specific scaling factors for the K_i values and with a more robust estimate of the transporter effect sizes still requires the inclusion of additional perpetrators and victims into a significantly larger DDI network for the involved transporters to achieve identifiability of both K_i values and the transporter effect size, given the non-specificity of transporter DDIs. As such, the effect of CsA as a perpetrator of RSV, MTX, and digoxin PK was adequately captured by the developed PBPK models. Because of the non-specificity of RSV, disentangling the contributions of individual transporter pathways in the RSV-CsA interaction is not feasible. Nonetheless, our findings were generally consistent with those of Lai et al. [7], who reported that genetic variation (single nucleotide polymorphisms) in drug transporters results in relatively small effects on plasma PK (usually less than three-fold). Furthermore, Lai et al. reported that polymorphisms of P-gp in Caucasian individuals resulted in increases in AUC of digoxin (0.25 mg) that ranged from 40 to 100%, whereas for BCRP, the resulting increase in the AUC of RSV (20 mg) ranged from 100 to 144%. In comparison, we predicted that a DDI with CsA would increase the AUC of MTX by approximately 30%, while that of digoxin would increase by 53%. For RSV, where multiple transporters are affected, the AUC increases by five-fold to eight-fold. Notably, the downstream effect of SNPs cannot be robustly quantified and is thus also subject to uncertainty [7].

The PK of CsA are known to be subject to strong inter-individual variability [43, 44]. Variations in activity or expression of protein binding (cholesterol levels), P-gp transport, CyP binding, red blood cell uptake (and haematocrit), and CYP3A4 metabolism, as well as the erratic dissolution profiles of its formulations, make it challenging to obtain a PBPK model consistent across all studies and populations [19, 21, 45]. The PBPK model presented here considers most

aspects, reflected in the prediction of both plasma and whole blood PK, and delivers a consensus model. As calculated in the parameter sensitivity analysis (ESM), lipophilicity is the most sensitive parameter in the model, followed by protein binding and CYP3A4 metabolism.

Both MTX and CsA PBPK models were initially established with input parameters derived from in vitro experiments. Similar to CsA, MTX PK data were obtained from various patient populations, which in turn introduced variability in the data used for model development. Nevertheless, the PBPK model could consistently characterise the plasma PK of MTX across all studies. For both models, adequate quantitative characterisation of metabolite PK enhanced confidence in the predictions. However, the underlying mechanisms for the underpredicted early time of onset of CsA metabolite remains an unresolved issue, but is unlikely to impact the accuracy of the simulated DDI with MTX. For MTX, the most sensitive parameters are related to its PO absorption (pH and solubility), protein binding and renal excretion.

The confidence in predicting DDIs for drug transporters is considered moderate in the scientific community [46]. Obtaining transporter expression levels and appropriate inhibition constants has been identified as the major challenge [47, 48]. The difficulty in the prediction of transporter-mediated DDIs can be caused by complicated membrane permeation processes (uptake and efflux/active transport and passive diffusion) based on the extended clearance concept [49]. Furthermore, the estimations of the passive diffusion/active transport ratio and the fraction of contribution of the DDI-target transporter are important for the accuracy of DDI prediction. The developed and used models described here use identical expression profiles of all involved enzymes or transporters across all use case scenarios. Equally, the K_i values for CsA (Table 1) have been scaled to a consistent value for both DDI scenarios with MTX and RSV. As a result, adequate characterisation of both DDIs of CsA with RSV and MTX were achieved.

Last, the model-predicted DDI for efflux transporters might depend on the selected luminal flow model, for example, traditional models (TMs) or segregated flow models (SFMs) [50]. SFMs describe a split flow pattern, with a lower flow rate (<20%) perfusing the active enterocyte region that houses the enzymes and absorptive/efflux transporters, and the remainder (>80%) perfusing the non-active serosal region [50–52]. The drug extraction ratio is slightly higher with the SFM as compared with the TM [50, 52]. This would imply that the predicted DDI with the TM potentially underpredicts the DDI with CsA, or results in a larger K_i scaling factor. However, BCRP is expressed in both the liver and intestine, as a result of which less definitive patterns emerge, and differences between the SFM and the TM are less certain [52]. Furthermore, SFMs are not available in PK-Sim (and neither in other commercial PBPK software [50]). The integration of SFMs as a part of future releases of these software should be considered to enable such DDIs to be better elucidated.

5 Conclusions

Overall, the presented work confirms a weak interaction potential for CsA with MTX, which is mediated through inhibition of AOX metabolism and BCRP-related active transport. Given that the interaction effect is not solely mediated through BCRP, as for the reference scenario with RSV, the effect size of the BCRP-related DDI requires further elucidation. In contrast to metabolic enzyme-mediated DDIs, transporter substrates lack specificity, making predictions of transporter-based DDIs more challenging [53]. The paucity of suitable data to train and validate these models compounds the challenge. Nevertheless, our work lays the foundation for the evaluation of DDIs mediated by the BCRP pathway. Unlike metabolism-based DDIs, wherein PBPK modelling can obviate the need for clinical DDIs in some cases, clinical DDI evaluation is required for transporters. Yet, mechanism-based DDI simulations can help to inform the design of these studies or to evaluate untested scenarios, such as a lower dose or an alternative dosing regimen. Being freely available in the Open Systems Pharmacology PBPK model repository, the models are available to the community for further development (https://www.open-systems-pharmacology.org).

Supplementary Information The online version contains supplementary material available at https://doi.org/10.1007/s40268-024-00495-1.

Acknowledgements Publication coordination was provided by John Gonzalez, PhD, of Galapagos NV (Mechelen, Belgium). Publications management support was provided by PharmaGenesis London, London, UK, funded by Galapagos NV.

Declarations

Funding This study was sponsored by Galapagos NV.

Conflicts of Interest/Competing Interests Stephan Schaller and Vanessa Baier are employees of esqLABS. Frederico Martins was an employee of esqLABS at the time of the work and is now an employee of Simulations Plus, Inc. Ingrid Michon was an employee of SGS Exprimo at the time of the work and is now an employee of Certara. Patrick Nolain was an employee of Galapagos at the time of the work and is now an employee of Novo Nordisk. Amit Taneja was an employee of Galapagos at the time of the work and owns subscription rights in the company, and is now an employee of Simulations Plus, Inc. esqLABS and SGS Exprimo are contract research organisations that were sponsored by Galapagos to conduct the study presented here.

Ethics Approval No ethical approval was required, as all data used in the article have been taken from publicly available sources.

Consent to Participate Not applicable.

Consent for Publication Not applicable.

Availability of Data and Material All available data used are included in the article (either referenced or in the tables).

Code Availability Not applicable.

Authors' Contributions All authors contributed to the study's conception and design. Material preparation, data collection and analysis were performed by SS, IM, VB, FM, PN and AT. The first draft of the manuscript was written by SS, and all authors commented on previous versions of the manuscript. All authors read and approved the final manuscript.

References

1. Waters NJ. Evaluation of drug-drug interactions for oncology therapies: in vitro-in vivo extrapolation model-based risk assessment. Br J Clin Pharmacol. 2015;79:946–58. https://doi.org/10.1111/bcp.12563.
2. Ishiguro A, Sato R, Nagai N. Development of a new Japanese guideline on drug interaction for drug development and appropriate provision of information. Drug Metab Pharmacokinet. 2020;35:12–7. https://doi.org/10.1016/j.dmpk.2019.11.009.
3. FDA Center for Drug Evaluation and Research. In vitro drug interaction studies: cytochrome P450 enzyme- and transporter-mediated drug interactions guidance for industry. 2020. Available from: hhttps://public4.pagefreezer.com/browse/FDA/15-09-2021T19:20/https:/www.fda.gov/regulatory-information/search-fda-guidance-documents/vitro-drug-interaction-studies-cytochrome-p450-enzyme-and-transporter-mediated-drug-interactions. https:/www.fda.gov/regulatory-information/search-fda-guidance-documents/vitro-drug-interaction-studies-cytochrome-p450-enzyme-and-transporter-mediated-drug-interactions. Accessed 18 Oct 2022.
4. EMA. Investigation of drug interactions. 2018. Available from: https://www.ema.europa.eu/en/investigation-drug-interactions. Accessed 18 Oct 2022.
5. Endres CJ, Hsiao P, Chung FS, Unadkat JD. The role of transporters in drug interactions. Eur J Pharm Sci. 2006;27:501–17. https://doi.org/10.1016/j.ejps.2005.11.002.
6. Mao Q, Unadkat JD. Role of the breast cancer resistance protein (BCRP/ABCG2) in drug transport—an update. AAPS J. 2015;17:65–82. https://doi.org/10.1208/s12248-014-9668-6.
7. Lai Y, Varma M, Feng B, Stephens JC, Kimoto E, El-Kattan A, et al. Impact of drug transporter pharmacogenomics on pharmacokinetic and pharmacodynamic variability: considerations for drug development. Expert Opin Drug Metab Toxicol. 2012;8:723–43. https://doi.org/10.1517/17425255.2012.678048.
8. Lee CA, O'Connor MA, Ritchie TK, Galetin A, Cook JA, Ragueneau-Majlessi I, et al. Breast cancer resistance protein (ABCG2) in clinical pharmacokinetics and drug interactions: practical recommendations for clinical victim and perpetrator drug-drug interaction study design. Drug Metab Dispos. 2015;43:490–509. https://doi.org/10.1124/dmd.114.062174.
9. Poirier A, Portmann R, Cascais A-C, Bader U, Walter I, Ullah M, et al. The need for human breast cancer resistance protein substrate and inhibition evaluation in drug discovery and development: why, when, and how? Drug Metab Dispos Biol Fate Chem. 2014;42:1466–77. https://doi.org/10.1124/dmd.114.058248.
10. US FDA. Drug development and drug interactions: table of substrates, inhibitors and inducers. 2020. Available from: https://www.fda.gov/drugs/drug-interactions-labeling/drug-development-and-drug-interactions-table-substrates-inhibitors-and-inducers#table3-2. [Accessed 18 Nov 2020].
11. Prueksaritanont T, Chu X, Evers R, Klopfer SO, Caro L, Kothare PA, et al. Pitavastatin is a more sensitive and selective organic anion-transporting polypeptide 1B clinical probe than rosuvastatin. Br J Clin Pharmacol. 2014;78:587–98. https://doi.org/10.1111/bcp.12377.
12. Peters SA. Physiologically based pharmacokinetic (PBPK) modeling and simulations: principles, methods, and applications in the pharmaceutical industry. Hoboken: Wiley; 2011.
13. Gerlowski LE, Jain RK. Physiologically based pharmacokinetic modeling: principles and applications. J Pharm Sci. 1983;72:1103–27. https://doi.org/10.1002/jps.2600721003.
14. Kuepfer L, Niederalt C, Wendl T, Schlender J-F, Willmann S, Lippert J, et al. Applied concepts in PBPK modeling: how to build a PBPK/PD model. CPT Pharmacomet Syst Pharmacol. 2016;5:516–31. https://doi.org/10.1002/psp4.12134.
15. Jones H, Rowland-Yeo K. Basic concepts in physiologically based pharmacokinetic modeling in drug discovery and development. CPT Pharmacomet Syst Pharmacol. 2013;2:e63. https://doi.org/10.1038/psp.2013.41.
16. Lohitnavy M, Lu Y, Lohitnavy O, Yang RSH. A physiologically-based pharmacokinetic model of methotrexate incorporating hepatic excretion via multidrug-resistance-associated protein 2 (Mrp2) in mice, rats, dogs, and humans. Annu Int Conf IEEE Eng Med Biol Soc. 2017;2017:2728–31. https://doi.org/10.1109/EMBC.2017.8037421.
17. Ogungbenro K, Aarons L, CRESim & Epi-CRESim Project Groups. Physiologically based pharmacokinetic modelling of methotrexate and 6-mercaptopurine in adults and children. Part 1: methotrexate. J Pharmacokinet Pharmacodyn. 2014;41:159–71. https://doi.org/10.1007/s10928-014-9354-4.
18. Bischoff KB, Dedrick RL, Zaharko DS, Longstreth JA. Methotrexate pharmacokinetics. J Pharm Sci. 1971;60:1128–33. https://doi.org/10.1002/jps.2600600803.
19. Jamei M, Bajot F, Neuhoff S, Barter Z, Yang J, Rostami-Hodjegan A, et al. A mechanistic framework for in vitro–in vivo extrapolation of liver membrane transporters: prediction of drug–drug interaction between rosuvastatin and cyclosporine. Clin Pharmacokinet. 2014;53:73–87. https://doi.org/10.1007/s40262-013-0097-y.
20. Thiel C, Schneckener S, Krauss M, Ghallab A, Hofmann U, Kanacher T, et al. A systematic evaluation of the use of physiologically based pharmacokinetic modeling for cross-species extrapolation. J Pharm Sci. 2015;104:191–206. https://doi.org/10.1002/jps.24214.
21. Zapke SE, Willmann S, Grebe S-O, Menke K, Thürmann PA, Schmiedl S. Comparing predictions of a PBPK model for

cyclosporine with drug levels from therapeutic drug monitoring. Front Pharmacol. 2021;12:1134. https://doi.org/10.3389/fphar.2021.630904.
22. Hanke N, Gómez-Mantilla JD, Ishiguro N, Stopfer P, Nock V. Physiologically based pharmacokinetic modeling of rosuvastatin to predict transporter-mediated drug-drug interactions. Pharm Res. 2021;38:1645–61. https://doi.org/10.1007/s11095-021-03109-6.
23. Open Systems Pharmacology Community. Open Systems Pharmacology. 2018. Available from: www.open-systems-pharmacology.org. [Accessed 4 Feb 2018].
24. Lippert J, Burghaus R, Edginton A, Frechen S, Karlsson M, Kovar A, et al. Open Systems Pharmacology community—an open access, open source, open science approach to modeling and simulation in pharmaceutical sciences. CPT Pharmacomet Syst Pharmacol. 2019;8:878–82. https://doi.org/10.1002/psp4.12473.
25. Rodgers T, Leahy D, Rowland M. Physiologically based pharmacokinetic modeling 1: predicting the tissue distribution of moderate-to-strong bases. J Pharm Sci. 2005;94:1259–76. https://doi.org/10.1002/jps.20322.
26. Boni FI, Almeida A, Lechanteur A, Sarmento B, Cury BSF, Gremião MPD. Mucoadhesive nanostructured polyelectrolytes complexes modulate the intestinal permeability of methotrexate. Eur J Pharm Sci. 2018;111:73–82. https://doi.org/10.1016/j.ejps.2017.09.042.
27. El-Sheikh AAK, Greupink R, Wortelboer HM, van den Heuvel JJMW, Schreurs M, Koenderink JB, et al. Interaction of immunosuppressive drugs with human organic anion transporter (OAT) 1 and OAT3, and multidrug resistance-associated protein (MRP) 2 and MRP4. Transl Res J Lab Clin Med. 2013;162:398–409. https://doi.org/10.1016/j.trsl.2013.08.003.
28. Wang Z, Zhang N, Chen C, Chen S, Xu J, Zhou Y, et al. Influence of the OATP polymorphism on the population pharmacokinetics of methotrexate in Chinese patients. Curr Drug Metab. 2019;20:592–600. https://doi.org/10.2174/1389200220666190701094756.
29. Abe T, Unno M, Onogawa T, Tokui T, Kondo TN, Nakagomi R, et al. LST-2, a human liver-specific organic anion transporter, determines methotrexate sensitivity in gastrointestinal cancers. Gastroenterology. 2001;120:1689–99. https://doi.org/10.1053/gast.2001.24804.
30. Anabtawi N, Drabison T, Hu S, Sparreboom A, Talebi Z. The role of OATP1B1 and OATP1B3 transporter polymorphisms in drug disposition and response to anticancer drugs: a review of the recent literature. Expert Opin Drug Metab Toxicol. 2022;18:459–68. https://doi.org/10.1080/17425255.2022.2113380.
31. Fox RI, Morgan SL, Smith HT, Robbins BA, Choc MG, Baggott JE. Combined oral cyclosporin and methotrexate therapy in patients with rheumatoid arthritis elevates methotrexate levels and reduces 7-hydroxymethotrexate levels when compared with methotrexate alone. Rheumatol Oxf Engl. 2003;42:989–94. https://doi.org/10.1093/rheumatology/keg277.
32. Basic anatomical and physiological data for use in radiological protection: reference values. A report of age- and gender-related differences in the anatomical and physiological characteristics of reference individuals. ICRP Publication 89. Ann ICRP. 2002;32:5–265.
33. Frechen S, Solodenko J, Wendl T, Dallmann A, Ince I, Lehr T, et al. A generic framework for the physiologically-based pharmacokinetic platform qualification of PK-Sim and its application to predicting cytochrome P450 3A4-mediated drug–drug interactions. CPT Pharmacomet Syst Pharmacol. 2021;10:633–44. https://doi.org/10.1002/psp4.12636.
34. Xia CQ, Liu N, Miwa GT, Gan L-S. Interactions of cyclosporin A with breast cancer resistance protein. Drug Metab Dispos. 2007;35:576–82. https://doi.org/10.1124/dmd.106.011866.
35. Elsby R, Martin P, Surry D, Sharma P, Fenner K. Solitary inhibition of the breast cancer resistance protein efflux transporter results in a clinically significant drug-drug interaction with rosuvastatin by causing up to a 2-fold increase in statin exposure. Drug Metab Dispos Biol Fate Chem. 2016;44:398–408. https://doi.org/10.1124/dmd.115.066795.
36. Gupta A, Dai Y, Vethanayagam RR, Hebert MF, Thummel KE, Unadkat JD, et al. Cyclosporin A, tacrolimus and sirolimus are potent inhibitors of the human breast cancer resistance protein (ABCG2) and reverse resistance to mitoxantrone and topotecan. Cancer Chemother Pharmacol. 2006;58:374–83. https://doi.org/10.1007/s00280-005-0173-6.
37. Reymond J-P, Steimer J-L, Niederberger W. On the dose dependency of Cyclosporin a absorption and disposition in healthy volunteers. J Pharmacokinet Biopharm. 1988;16:331–53. https://doi.org/10.1007/BF01062550.
38. Simonson SG, Raza A, Martin PD, Mitchell PD, Jarcho JA, Brown CDA, et al. Rosuvastatin pharmacokinetics in heart transplant recipients administered an antirejection regimen including cyclosporine. Clin Pharmacol Ther. 2004;76:167–77. https://doi.org/10.1016/j.clpt.2004.03.010.
39. Hanke N, Frechen S, Moj D, Britz H, Eissing T, Wendl T, et al. PBPK models for CYP3A4 and P-gp DDI prediction: a modeling network of rifampicin, itraconazole, clarithromycin, midazolam, alfentanil, and digoxin. CPT Pharmacomet Syst Pharmacol. 2018;7:647–59. https://doi.org/10.1002/psp4.12343.
40. Dorian P, Strauss M, Cardella C, David T, East S, Ogilvie R. Digoxin-cyclosporine interaction: severe digitalis toxicity after cyclosporine treatment. Clin Investig Med Med Clin Exp. 1988;11:108–12.
41. Liu S-G, Gao C, Zhang R-D, Zhao X-X, Cui L, Li W-J, et al. Polymorphisms in methotrexate transporters and their relationship to plasma methotrexate levels, toxicity of high-dose methotrexate, and outcome of pediatric acute lymphoblastic leukemia. Oncotarget. 2017;8:37761–72. https://doi.org/10.18632/oncotarget.17781.
42. Tornio A, Filppula AM, Niemi M, Backman JT. Clinical studies on drug–drug interactions involving metabolism and transport: methodology, pitfalls, and interpretation. Clin Pharmacol Ther. 2019;105:1345–61. https://doi.org/10.1002/cpt.1435.
43. Méndez A, Monforte V, Berastegui C, López-Meseguer M, Bravo C, Pou L, et al. High intra-individual variability of cyclosporine pharmacokinetics in lung transplant recipients without cystic fibrosis. Clin Transplant. 2014;28:743–8. https://doi.org/10.1111/ctr.12371.
44. Lindholm A, Henricsson S, Lind M, Dahlqvist R. Intraindividual variability in the relative systemic availability of cyclosporin after oral dosing. Eur J Clin Pharmacol. 1988;34:461–4. https://doi.org/10.1007/BF01046702.
45. Ptachcinski RJ, Venkataramanan R, Burckart GJ, Gray JA, Van Thiel DH, Sanghvi A, et al. Cyclosporine kinetics in healthy volunteers. J Clin Pharmacol. 1987;27:243–8. https://doi.org/10.1002/j.1552-4604.1987.tb02193.x.
46. Wagner C, Zhao P, Pan Y, Hsu V, Grillo J, Huang SM, et al. Application of physiologically based pharmacokinetic (PBPK) modeling to support dose selection: report of an FDA public workshop on PBPK. CPT Pharmacomet Syst Pharmacol. 2015;4:226–30. https://doi.org/10.1002/psp4.33.
47. Jones H, Chen Y, Gibson C, Heimbach T, Parrott N, Peters S, et al. Physiologically based pharmacokinetic modeling in drug discovery and development: a pharmaceutical industry perspective. Clin Pharmacol Ther. 2015;97:247–62. https://doi.org/10.1002/cpt.37.

48. Taskar KS, Pilla Reddy V, Burt H, Posada MM, Varma M, Zheng M, et al. Physiologically-based pharmacokinetic models for evaluating membrane transporter mediated drug–drug interactions: current capabilities, case studies, future opportunities, and recommendations. Clin Pharmacol Ther. 2020;107:1082–115. https://doi.org/10.1002/cpt.1693.
49. Watanabe T, Kusuhara H, Sugiyama Y. Application of physiologically based pharmacokinetic modeling and clearance concept to drugs showing transporter-mediated distribution and clearance in humans. J Pharmacokinet Pharmacodyn. 2010;37:575–90. https://doi.org/10.1007/s10928-010-9176-y.
50. Pang KS, Peng HB, Noh K. The segregated intestinal flow model (SFM) for drug absorption and drug metabolism: implications on intestinal and liver metabolism and drug–drug interactions. Pharmaceutics. 2020;12:312. https://doi.org/10.3390/pharmaceutics12040312.
51. Chow ECY, Pang KS. Why we need proper PBPK models to examine intestine and liver oral drug absorption. Curr Drug Metab. 2013;14:57–79.
52. Pang KS, Han YR, Noh K, Lee PI, Rowland M. Hepatic clearance concepts and misconceptions: why the well-stirred model is still used even though it is not physiologic reality? Biochem Pharmacol. 2019;169: 113596. https://doi.org/10.1016/j.bcp.2019.07.025.
53. Zamek-Gliszczynski MJ, Taub ME, Chothe PP, Chu X, Giacomini KM, Kim RB, et al. Transporters in drug development: 2018 ITC recommendations for transporters of emerging clinical importance. Clin Pharmacol Ther. 2018;104:890–9. https://doi.org/10.1002/cpt.1112.
54. el Tayar N, Mark AE, Vallat P, Brunne RM, Testa B, van Gunsteren WF. Solvent-dependent conformation and hydrogen-bonding capacity of cyclosporin A: evidence from partition coefficients and molecular dynamics simulations. J Med Chem. 1993;36:3757–64. https://doi.org/10.1021/jm00076a002.
55. Poulin P, Theil F-P. Prediction of pharmacokinetics prior to in vivo studies. 1. Mechanism-based prediction of volume of distribution. J Pharm Sci. 2002;91:129–56. https://doi.org/10.1002/jps.10005.
56. Czogalla A. Oral cyclosporine A—the current picture of its liposomal and other delivery systems. Cell Mol Biol Lett. 2009;14:139–52. https://doi.org/10.2478/s11658-008-0041-6.
57. Chiu SHL, Green ML, Baylis FP, Eline D, Rosegay A, Meriwether H, et al. Absorption, tissue distribution, and excretion of tritium-labeled ivermectin in cattle, sheep, and rat. J Agric Food Chem. 1990;38:2072–8. https://doi.org/10.1021/jf00101a015.
58. Fahr A. Cyclosporin clinical pharmacokinetics. Clin Pharmacokinet. 1993;24:472–95. https://doi.org/10.2165/00003088-199324060-00004.
59. Legg B, Rowland M. Cyclosporin: measurement of fraction unbound in plasma. J Pharm Pharmacol. 1987;39:599–603. https://doi.org/10.1111/j.2042-7158.1987.tb03436.x.
60. Dai Y, Iwanaga K, Lin YS, Hebert MF, Davis CL, Huang W, et al. In vitro metabolism of cyclosporine A by human kidney CYP3A5. Biochem Pharmacol. 2004;68:1889–902. https://doi.org/10.1016/j.bcp.2004.07.012.
61. Zheng S, Tasnif Y, Hebert MF, Davis CL, Shitara Y, Calamia JC, et al. CYP3A5 gene variation influences cyclosporine A metabolite formation and renal cyclosporine disposition. Transplant J. 2013;95:821–7. https://doi.org/10.1097/TP.0b013e31827e6ad9.
62. Choughule KV, Joswig-Jones CA, Jones JP. Interspecies differences in the metabolism of methotrexate: an insight into the active site differences between human and rabbit aldehyde oxidase. Biochem Pharmacol. 2015;96:288–95. https://doi.org/10.1016/j.bcp.2015.05.010.
63. Fricker G, Drewe J, Huwyler J, Gutmann H, Beglinger C. Relevance of p-glycoprotein for the enteral absorption of cyclosporin A: in vitro-in vivo correlation. Br J Pharmacol. 1996;118:1841–7. https://doi.org/10.1111/j.1476-5381.1996.tb15612.x.
64. Breedveld P, Pluim D, Cipriani G, Dahlhaus F, van Eijndhoven MAJ, de Wolf CJF, et al. The effect of low pH on breast cancer resistance protein (ABCG2)-mediated transport of methotrexate, 7-hydroxymethotrexate, methotrexate diglutamate, folic acid, mitoxantrone, topotecan, and resveratrol in in vitro drug transport models. Mol Pharmacol. 2007;71:240–9. https://doi.org/10.1124/mol.106.028167.
65. Chen J, Veras MMS, Liu C, Lin J. Methotrexate for ankylosing spondylitis. Cochrane Database Syst Rev. 2013. https://doi.org/10.1002/14651858.CD004524.pub4.
66. Costales C, Lin J, Kimoto E, Yamazaki S, Gosset JR, Rodrigues AD, et al. Quantitative prediction of breast cancer resistant protein mediated drug-drug interactions using physiologically-based pharmacokinetic modeling. CPT Pharmacomet Syst Pharmacol. 2021;10:1018–31. https://doi.org/10.1002/psp4.12672.
67. Tiberghien F, Wenandy T, Loor F. The potent immunosuppressive cyclosporin FR901459 inhibits the human P-glycoprotein and formyl peptide receptor functions. J Antibiot (Tokyo). 2000;53:509–15. https://doi.org/10.7164/antibiotics.53.509.
68. Ho RH, Tirona RG, Leake BF, Glaeser H, Lee W, Lemke CJ, et al. Drug and bile acid transporters in rosuvastatin hepatic uptake: function, expression, and pharmacogenetics. Gastroenterology. 2006;130:1793–806. https://doi.org/10.1053/j.gastro.2006.02.034.
69. Bannwarth B, Péhourcq F, Schaeverbeke T, Dehais J. Clinical pharmacokinetics of low-dose pulse methotrexate in rheumatoid arthritis. Clin Pharmacokinet. 1996;30:194–210. https://doi.org/10.2165/00003088-199630030-00002.
70. Lim M, Seong SJ, Park J, Seo JJ, Lee J, Yu K-S, et al. Assessment of pharmacokinetic proportionality of levofloxacin and cyclosporine over a 100-fold dose range in healthy human volunteers. Expert Opin Drug Metab Toxicol. 2012;8:399–405. https://doi.org/10.1517/17425255.2012.666237.